NeuroImage: Clinical 24 (2019) 102090

Contents lists available at ScienceDirect

NeuroImage: Clinical

journal homepage: www.elsevier.com/locate/ynicl

Differential involvement of rubral branches in chronic capsular and pontine stroke

Guo Jun[a,b,c], Liu Jingchun[a,b], Wang Caihong[d], Cao Chen[c], Fu Lejun[a,b,c], Han Tong[c], Cheng Jingliang[d], Yu Chunshui[a,b], Qin Wen[a,b,*]

[a] Department of Radiology, Tianjin Medical University General Hospital, Tianjin 300052, China
[b] Tianjin Key Laboratory of Functional Imaging, Tianjin Medical University General Hospital, Tianjin 300052, China
[c] Department of Radiology, Tianjin Huanhu Hospital, Tianjin 300350, China
[d] Department of Magnetic Resonance Imaging, The First Affiliated Hospital of Zhengzhou University, Zhengzhou 450052, China

ARTICLE INFO

Keywords:
Corticorubral tracts
Dentatorubral tracts
Rubrospinal tracts
Pontine stroke
Capsular stroke
Diffusion tensor imaging

ABSTRACT

Background and Purpose: Early studies have indicated that the cortico-rubro-spinal tracts play important roles in motor dysfunction after stroke. However, the differential involvement of the rubral branches in capsular and pontine stroke, and their associations with the motor impairment are still unknown.

Methods: The present study recruited 144 chronic stroke patients and 91 normal controls (NC) from three hospitals, including 102 cases with capsular stroke (CS) and 42 cases with pontine stroke (PS). The rubral branches, including bilateral corticorubral tracts (CRT), dentatorubral tracts (DRT), and rubrospinal tracts (RST), and the cortico-spinal tract (CST) were reconstructed based on the dataset of the Human Connectome Project. Group differences in diffusion scalars of each rubral branch were compared, and the associations between the diffusion measures of rubral branches and the Fugl-Meyer assessment (FMA) scores were tested.

Results: The bilateral CRT of the CS cases showed significantly lower factional anisotropy (FA) than in the NC. The bilateral DRT of the PS cases had lower FA than in the NC. Both CS and PS cases had significantly lower FA of the bilateral RST than the NC. Besides, the stroke patients demonstrated significantly lower FA in bilateral CSTs than the NC. Partial correlation analysis identified significantly positive correlations between the FA of the ipsilesional and CRT and the FMA scores in the CS group, and significantly positive correlations between the FA of the RST bilaterally and the FMA scores in the CS and PS groups. Furthermore, the association between RST integrity and FMA scores still survived after controlling for the effect of the CST. Finally, multiple regression modelling found that rubral tract FA explained 39.2% of the variance in FMA scores for CS patients, and 48.8% of the variance in FMA scores for PS patients.

Conclusions: The bilateral rubral branches were differentially involved in the chronic capsular and pontine stroke, and the impairment severity of each rubral branch was dependent on lesion locations. The integrity of the rubral branches is related to motor impairment in both the chronic capsular and pontine stroke.

AD = axial diffusivity
CRT = corticorubral tract
CS = capsular stroke
CST = corticospinal tract
DRT = dentatorubral tract
DSI = diffusion spectrum imaging
DTI = diffusion tensor imaging
FA = fractional anisotropy
FMA = Fugl-Meyer Assessment
FWE = Family-wise error
FDR = False-discovery rate
HCP = Human Connectome Project
NC = normal control
PS = pontine stroke
RD = radial diffusivity
ROI = region of interest
RST = rubrospinal tracts

1. Introduction

The red nucleus is a key relay that links the cerebral cortex, cerebellum and the spinal cord; it receives projections from the cerebral

* Corresponding author at: Department of Radiology, Tianjin Medical University General Hospital, No. 154, Anshan Road, Heping District, Tianjin 300052, China.
E-mail address: wayne.wenqin@gmail.com (W. Qin).

https://doi.org/10.1016/j.nicl.2019.102090
Received 10 July 2019; Received in revised form 6 November 2019; Accepted 10 November 2019
Available online 12 November 2019

cortex through the corticorubral tracts (CRT), and projections from the dentate nucleus(DN) of the cerebellum through the dentatorubral tracts (DRT) (Cacciola et al., 2019), and yields efferents to the interneurons and motor neurons of the spinal cord through the rubrospinal tracts (RST) (Lemon, 2016; Milardi et al., 2016). In vivo studies using diffusion tensor imaging (DTI) reconstruct the connections between the red nucleus and the ipsilateral cerebral cortex, thalamus and contralateral cerebellar dentate nucleus (Habas and Cabanis, 2006, 2007; Meola et al., 2016). However, in traditional DTI, it is hard to resolve the cross-fiber in rubral pathways, such as the decussating fibers of the DRT and RST, thus making it hard to reconstruct the full branches of the rubral pathways.

The structural integrity of corticospinal tracts (CST) is closely related to the degree of motor dysfunction and recovery after stroke (Lotze et al., 2012; Schaechter et al., 2009; Sterr et al., 2010; Stinear et al., 2007). Moreover, some studies have indicated that the cortico-rubro-spinal tracts play important roles in motor dysfunction and recovery after stroke (Kim et al., 2018; Ruber et al., 2012; Siegel et al., 2015; Yeo and Jang, 2010). However, it remains unknown whether the rubral branches are differentially involved in the stroke, which is important for understanding the roles of each rubral branch in stroke-induced disability and recovery. Early studies have also shown that the lesion locations of stroke were closely associated with the types and severity of dysfunction and recovery potentials (Cheng et al., 2014); moreover, different infarction location can induce differential types of structural damage and reorganization of brain gray matter, even in brain regions outside of the lesion (Jiang et al., 2017). Thus, it also interesting to elucidate whether the patterns of damage/reorganization of the rubral branches are also lesion-location dependent.

Because the brain regions with changed gray matter are connected by the deep white matter tracts, the gray matter changes outside the lesion (Jiang et al., 2017) might be the secondary to the changes of their connected white matter. Thus, we hypothesized that patients with capsular stroke (CS) and pontine stroke (PS) may induce differential structural damage and reorganization along each branch of the rubral pathway, which may account for the residual motor impairment at the chronic stage. To validate our hypothesis, we recruited a relatively large sample size of unilateral chronic stroke patients (including 102 cases with CS and 42 with PS) and normal controls (NC). Benefit from the large sample size of recruited patients, we separately analyzed and reported the findings with left- and right-side lesions to validate the reproducibility of our findings. Because the infarct lesions may destruct the continuity of rubral branches, causing the tractography failed, we reconstruct the group-wise probabilistic fibers of each branch from a large sample of healthy adults and applied them to the candidate cohort to obtain the precise rubral branches. Specifically, we reconstructed individual branches of rubral pathways (including the CRT, DRT and RST) using multi-shell diffusion data collected by the Human Connectome Project (HCP). The HCP acquires and shares high quality human magnetic resonance (MR) imaging data for researches (Van Essen et al., 2013). For example, diffusion weighted MR data were collected with high spatial resolution (1.25 -mm^3) and high-angular resolution (270+ diffusion directions). In combination with state-of-the-art reconstruction algorithms, it is hoped to dramatically improve the resolution for cross-fibers along the rubral pathways (Sotiropoulos et al., 2013; Ugurbil et al., 2013). Based on the reconstructed rubral pathways, we then tried to investigate the microstructural changes along the rubral branches in chronic CS and pontine stroke PS in a voxel-wise manner, and tried to associate the involvement of the rubral branches with the severity of motor impairment.

2. Materials and methods

The authors declare that all supporting data are available within the article and its online Supplemental files.

2.1. Participants

In the present study, 144 chronic stroke patients and 91 normal controls were recruited for this study from three hospitals, including 102 cases with CS and 42 with PS. Normal controls were matched to the stroke patients for gender and age. This research was approved by the ethics committee of local medical institutions. All participants signed informed consent forms prior to the study. The enrollment criteria for patients were as follows: (1) first-onset ischemic stroke; (2) demonstrated motor dysfunction at the initial inpatient; (3) initial CT or MR imaging identified a single lesion involving the posterior limbs of the internal capsule for the CS; or a single lesion at the level of the unilateral pons for the PS;(4) the interval between stroke onset and enrollment was longer than 6 months; and (5) the age was range 40–80 years. The exclusion criteria were as follows: (1) patients with recurrent cerebral infarction; (2) left-handedness before stroke; (3) a history of drug dependence or psychiatric disorders; (4) other intracranial lesions, such as tumors, vascular malformations, cerebral hemorrhage, etc.; (5) poor image quality; and (6) cannot complete neurological and MR examinations. All patients underwent Fugl-Meyer assessment (FMA),

Table 1
Demographic and clinical data of patients with stroke and control subjects.

	Capsular stroke	Pontine stroke	Normal controls	Statistics	P value
Patients with left lesions					
Age(year)	43–75(55.65 ± 8.07)	49–69(58.48 ± 6.14)	40–75(55.54 ± 7.63)	$F = 1.325$	0.269
Gender (Male/Female)	39/10	13/8	47/40	$\chi^2 = 8.811$	0.012
No. of patients for each scanner (Trio Tim/ MR750/MR750)	9/23/17	5/9/7	26/34/27	$\chi^2 = 2.258$	0.689
FMA total	19–100(92.19 ± 18.90)	12–100(90.05 ± 23.49)	/	$t = 0.401$	0.689
FMA upper extremity	10–66(60.13 ± 14.55)	9–66(59.10 ± 16.29)	/	$t = 0.261$	0.795
FMA lower extremity	9–34(32.06 ± 5.02)	3–34(30.95 ± 7.47)	/	$t = 0.725$	0.471
Timing of follow-up imaging (days)	185–2099(609.0 ± 404.1)	181–1018(473.9 ± 253.7)	/	$t = 1.414$	0.162
Lesion volume at Chronic stage(ml)	0.01–3.73(0.71 ± 0.85)	0.02–0.73(0.21 ± 0.21)	/		/
Patients with right lesions					
Age(year)	41–71(56.78 ± 6.93)	42–72(57.12 ± 8.99)	40–75(55.54 ± 7.63)	$F = 0.561$	0.572
Gender (Male/Female)	26/18	11/6	47/40	$\chi^2 = 0.800$	0.670
No. of patients for each scanner (Trio Tim/ MR750/MR750)	14/14/16	3/6/8	26/34/27	$\chi 2 = 2.423$	0.666
FMA total	28–100(87.89 ± 21.79)	65–100(93.35 ± 10.11)	/	$t = -1.334$	0.188
FMA upper extremity	3–66(56.91 ± 17.06)	42–66(61.88 ± 6.74)	/	$t = -1.632$	0.108
FMA lower extremity	15–34(30.75 ± 5.98)	23–34(31.47 ± 3.61)	/	$t = -0.574$	0.569
Timing of follow-up imaging (days)	216–1612(537.1 ± 286.3)	204–1075(479.9 ± 276.9)	/	$t = 0.706$	0.483
Lesion volume at Chronic stage(ml)	0.04–5.62(0.78 ± 1.14)	0.02–0.38(0.13 ± 0.10)	/	/	

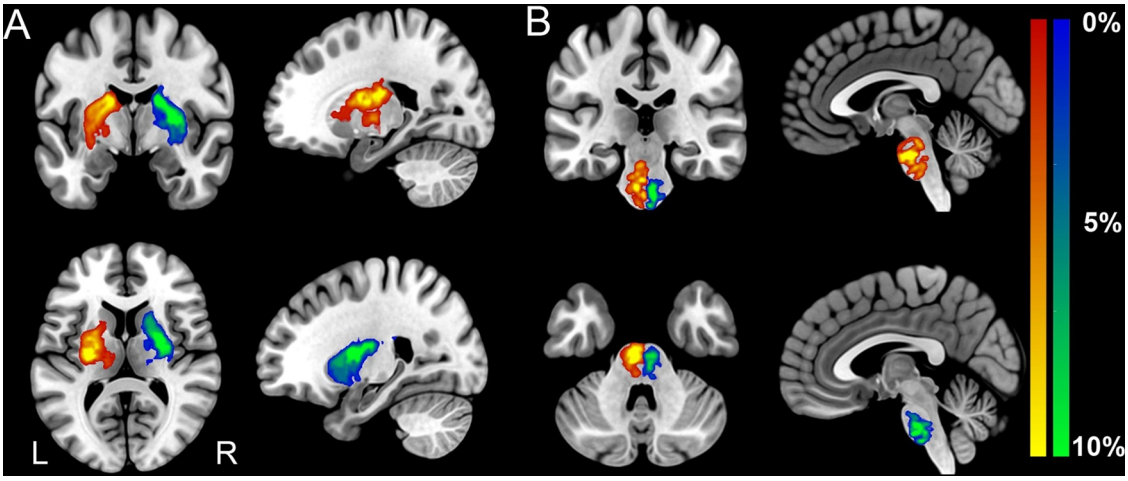

Fig. 1. Probability maps of stroke lesions. (A) Capsular stroke (B) Pontine stroke. The color bar represents the lesion probability across patients.(For interpretation of the references to colour in this figure legend, the reader is referred to the web version of this article.)

which is frequently used to evaluate the motor impairment in clinical practice. The detailed demographic and clinical data are described in Table 1.

2.2. MR data acquisition

2.2.1. Stroke dataset

MR images (MRI) were acquired using three 3.0T MR scanners from three hospitals, including a Magnetom Trio Tim MR scanner (Siemens, Erlangen, Germany) and two Discovery MR750 scanners (GE Healthcare).

For the Trio Tim scanner, 3D T1-weighted (T1W) images were acquired using the magnetization prepared rapid acquisition gradient echo (MPRAGE) sequence with the following parameters: repetition time (TR)/ echo time (TE) /inversion time (TI) = 2000/2.26/900 ms, flip angle = 9°, field of view (FOV) = 256 mm × 232 mm, matrix = 256 × 232, thickness = 1 mm, and slices = 192, resulting in a 1 mm isotropic voxel; diffusion MRI (dMRI) images were acquired using single-shot spin-echo planar imaging (SS-SE-EPI) sequence with the following parameters: TR/TE = 6000/85 ms, flip angle = 90°, FOV = 256 mm × 256 mm, matrix = 128 × 128, thickness = 3 mm, gap = 0, slices = 45, number of none-diffusion volumes = 1; and 64 diffusion directions with b = 1000 s/mm^2.

For the MR750 scanners, 3D T1-weighted images were acquired using the brain volume (BRAVO) sequence with the following parameters: TR/TE/TI = 8.14/3.17/450 ms, flip angle =12°, FOV = 256 mm × 256 mm, matrix = 256 × 256, thickness = 1 mm, slices =188, voxel size = 1 mm × 1 mm × 1 mm; dMRI images were acquired using the SS-SE-EPI sequence with the following parameters: TR/TE = 7100/60.5 ms, flip angle = 90°, FOV = 256 mm × 256 mm, matrix = 128 × 128, thickness = 2 mm, gap = 0, slices = 70, number of no diffusion volumes = 10; 64 diffusion directions with b = 1000 s/mm^2. All subjects were informed to close their eyes and to be motionless during the scanning.

2.2.2. HCP dataset

The HCP dataset was obtained using the 3.0T WU-Minn-Ox HCP scanner with very strong magnetic field gradients (100 mT/m) along with new and optimized dMRI pulse sequences (Glasser et al., 2016). The 3D T1W images were obtained using the MPRAGE sequence with the following parameters: TR/TE/TI =2400/2.14/1000 ms, flip angle =8°, FOV =224 mm × 224 mm, matrix = 320 × 320, and slice thickness =0.7 mm, resulting in a 0.7 mm isotropic voxel. The diffusion images were obtained using a multi-band SS-SE-EPI sequence with the following parameters: TR/TE =5520/89.5 ms, flip angle =78°, multi-band factor=3, FOV = 210 mm × 180 mm, matrix = 168 × 144, and slice thickness=1.25 mm, resulting in a 1.25 mm isotropic voxel. The diffusion session includes 6 runs, representing 3 different gradient tables, which correspond to 3 shells of b = 1000, 2000, and 3000 s/mm^2, and each table acquired once with right-to-left and left-to-right phase encoding directions, respectively. Each gradient table includes approximately 90 diffusion weighting directions plus 6 b = 0 acquisitions interspersed throughout each run. (http://protocols.humanconnectome.org/HCP/3T/imaging-protocols.html)

2.3. Data processing

2.3.1. Stroke dataset

The image quality was first checked manually, and we excluded some subjects due to poor quality DTI images, including 11 cases with motion artifacts, 3 cases without T1 images, and 3 cases with severe distortion caused by dentures. Finally, our study included 93 cases with CS and 38 with PS and 87 normal controls.

The dMRI were preprocessed on the FSL 5.0.10 platform (https://fsl.fmrib.ox.ac.uk/fsl/fslwiki/). First, the eddy current and susceptibility- induced image distortion and head motion-induced displacement were corrected using the "eddy current correction tool" implemented in the FSL. Then, the brain tissues were extracted using the "brain extraction tool v2.1″, which generates a non-diffusion (b0) brain volume and mask. Then, a linear least square algorithm was used to fit the diffusion tensor model at each voxel, and the fractional anisotropy (FA) was calculated based on the decomposed eigenvalues of the diffusion tensor, which quantifies the extent of diffusion anisotropy and is broadly used to identify the microstructural properties of brain white matter (Qin et al., 2012; Ruber et al., 2012). The FA maps were then normalized into the Montreal Neurological Institute (MNI) space along the following: first, non-diffusion b0 brain images were linearly coregistered with the T1W brain images; then, the T1 images were segmented into different tissue components and were normalized into the MNI space using diffeomorphic anatomical registration through exponentiated lie algebra (DARTEL) algorithms; finally, the deformation parameters of the preceding two-steps were concatenated and used to write the native FA map of each subject into the MNI space. Finally, the normalized FA maps were smoothed with full width at half maximum (FWHM) of 8 × 8 × 8 mm^3. Probability maps of lesion distribution in patients with CS and PS are shown in Fig. 1.

2.3.2. HCP-dataset

The downloaded diffusion HCP data had been preprocessed based on minimal preprocessing pipelines (Glasser et al., 2013), which

included b0 intensity normalization, EPI distortion correction (topup toolbox), subject motion correction (eddy toolbox), gradient non-linearity correction, b0 to T1W linear registration, etc.(http://dsi-studio.labsolver.org/Manual/Parse-DICOM). The T1W images were first segmented into different tissue components and were normalized into the MNI space using DARTEL algorithms, and the diffusion-to-MNI deformation parameters were calculated by concatenating the two preceding registration steps (i.e., b0-to-T1W and T1W-to-MNI).

The orientation diffusion function (ODF) of each voxel was fitted using generalized q-sampling imaging (GQI) algorithm. GQI estimates the spin distribution function directly from diffusion MR signals that can reliably resolve multiple fiber orientations within one single voxel (Yeh et al., 2013; Yeh FC, 2010), thus it is far better than traditional tensor-based tractography methods in resolving cross fibers such as the rubral branches. In the ISMRM 2015 Tractography challenge, GQI-based tractography has achieved the highest valid connections (92%) among 96 fiber tracking methods (Maier-Hein et al., 2017). The parameters for ODF fitting included: diffusion sampling length ratio = 1.25, ODF decomposition fraction = 0.05 (Yeh et al., 2013). Subsequently, we performed deterministic tractography to reconstruct the branches of rubral pathways using the streamline method. The red nucleus was chosen as the endpoint region of interest (ROI) of fibers. The ROI was drawn on b0 images of each subject since the boundaries of red nuclei can be clearly identified on them (Fig. 2A). In the present study, we initially enrolled 100 subjects from the HCP dataset, in which 89 participants were selected to track the rubral pathway according to the following two principles: (1) the boundary of each red nucleus can be clearly displayed and drawn; and (2) the sizes of the bilateral red nuclei are comparable. The ROI of the red nuclei on each side of each subject was manually drawn by a radiologist with 18 years of professional skills using MRIcron software (www.nitrc.org/projects/mricron). The parameters for fiber tracking were as follows: 1,000,000 seeds were randomly placed at the voxel of the whole brain, angular threshold = 60°, step size = 0.62 mm, termination threshold for quantitative anisotropy = 0.08, and fiber trajectories were smoothed by averaging the propagation direction with 20% of the previous direction.

The fiber bundles that end in the red nuclei were further manually trimmed by the same radiologist using the fiber bundle editing tool in DSI Studio to remove pseudo-fibers. Then, three fiber bundles on each side were isolated based on their terminating/pass regions, including the CRT that terminates at the cerebral cortex, the DRT that terminates at the dentate, and the RST that prolongates to the medulla (Fig. 2B).

The seeds for CST reconstruction were manually defined at each subject, including the primary motor cortex (termination seeds), posterior limb of internal capsule (pass seeds), and cerebral peduncle (pass seeds). Fibers that terminate or pass through all the three ipsilateral seeds were reconstructed using the same tractography algorithm and parameters as described in rubral branches tractography.

The three pairs of rubral branches and the CSTs were then normalized into the MNI space using the diffusion-to-MNI deformation parameters. Finally, a group-level fiber probabilistic map of each fiber bundle was calculated by averaging the normalized fibers of all subjects

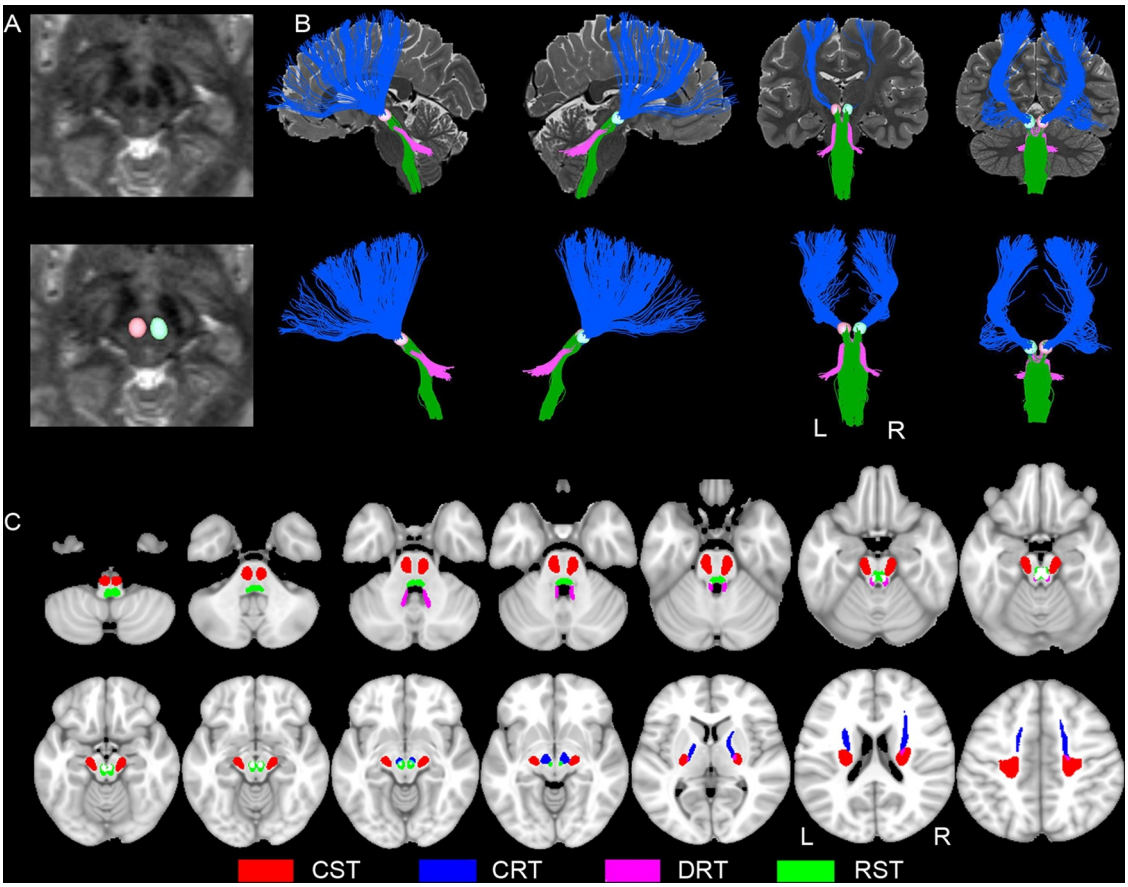

Fig. 2. Rubral branches and CST reconstructed based on HCP dMRI data. (A) The seeds of red nuclei were defined based on b0 images. (B) An example of rubral branches reconstructed by the GQI algorithm, which included the CRT (blue), DRT (pink), and RST (green). The CRT ascends from the red nucleus to the internal capsule, and terminates into the prefrontal-parietal cortex. The DRT descends from the red nucleus to the ipsilateral cerebral peduncle, crosses the middle line, and terminates into the contralateral dentate via the superior cerebellar peduncle. The RST descends from the red nucleus to the dorsal part of the bilateral midbrain, pons, and medulla. (C) Probabilistic map (25%) of each rubral branch and corticospinal tract (red). Abbreviations: CRT = corticorubral tracts, CST = corticospinal tract, dMRI = diffusion magnetic resonance imaging, DRT = dentatorubral tracts, HCP = Human Connectome Project, RST = rubrospinal tracts.(For interpretation of the references to colour in this figure legend, the reader is referred to the web version of this article.)

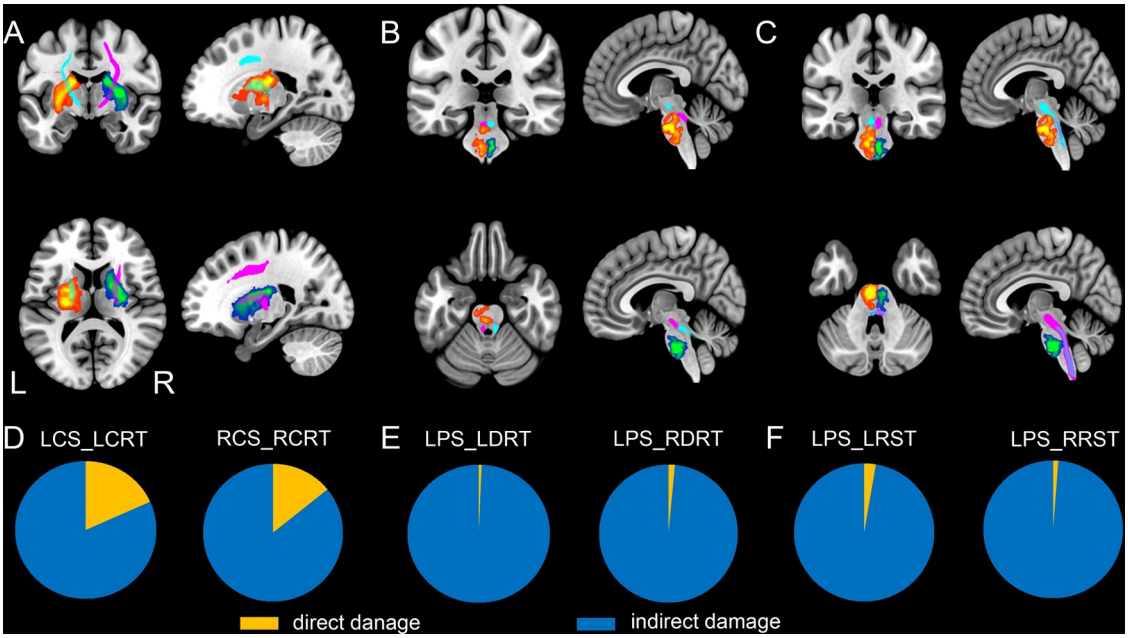

Fig. 3. Spatial relationships between lesion locations and rubral branches. (A) The relationship between CS lesions (left lesion: warm, right lesion: cool) and CRT, (B) between PS lesions and DRT, and (C) between PS lesions and RST (left tract: cyan, right tract: violet). Percentage of direct (orange) and indirect damage (blue) of the CRT (D), DRT (E), and RST (F) was shown in the bottom panel. Abbreviations: CRT = corticorubral tracts, CS = capsular stroke, DRT = dentatorubral tracts, PS = pontine stroke, RST = rubrospinal tracts.(For interpretation of the references to colour in this figure legend, the reader is referred to the web version of this article.)

(Fig. 2C). The tractography was conducted using DSI Studio 2017 build (http://dsi-studio.labsolver.org).

2.4. Statistical analyses

To identify potential microstructural changes of the rubral branches and CST after chronic CS and PS, a voxel-wise general linear model (GLM) was carried out with groups (CS, PS and NC) as the fixed effects, and age and gender nuisance covariates within each fiber mask independently, using SPM 12 (https://www.fil.ion.ucl.ac.uk/spm/software/spm12/). According to a recent study showing that systematic bias of FA cannot be ignored in multicenter studies, different scanners were also considered as random nuisance covariates in the GLM model (Teipel et al., 2011). The fiber mask was created by thresholding the group-level fiber probabilistic map higher than 25% and binarizing the non-zero voxels. We chose this threshold because we found that a lower threshold would cause a non-specific distribution of the rubral branches, while a higher threshold would disrupt fiber continuity between the cortex and red nuclei. Multiple comparisons were corrected using a cluster-level family-wise error (FWE) method (peak-wise $P < 0.001$, corrected cluster-wise $P < 0.05$).

The mean FA, axial diffusivity (AD) and radial diffusivity (RD) of clusters with significant differences in each tract were extracted, and ROI-wise post hoc analyses were carried out using the GLM model in the PASW statistics 19 software (https://www.ibm.com/analytics/spss-statistics-software) to compare group differences in these diffusion scalars between each pair of groups. The false discovery rate (FDR) method was used to correct for multiple comparisons ($q < 0.05$). To test the associations of the microscopic integrity of each tract with the motor impairment, partial correlation analyses (controlling for the effects of age, gender, and scanners) were performed to test the associations between the FA values of all tracts (including the CST and three rubral branches) and the FMA scores. Finally, to further elucidate whether the integrity of the rubral branches contributes independently to the residual motor impairment that is irrespective of the CST, the FA values of ipsilesional CST in combination with the former covariates (age, gender, and scanners) were regressed out in the correlations between the FA of each rubral branch and the FMA scores ($q < 0.05$, FDR correction).

To evaluate the power of the integrity of rubral branches on explaining the individual variance in severity of motor impairment, we additionally introduce a multiple regression model with the total FMA score as the dependent variable, and the FA value of the bilateral DRT and RST, and that of ipsilesional CRT as the explained variables (features). We did not introduce the FA of contralesional CRT as the explained variable because this tract was only involved in patients with left lesion while not in whom with right lesion, and there is no association between the FMA and FA of the contralesional CRT (see Supplementary Datasheet 1). Before model estimation, the effects of age, gender, and scanners were regressed out from each feature, and each feature was then scaled into normal distribution with mean of 0 and standard deviation of 1 using Gaussian replacement method. A F-test was used to evaluate the statistical significance ($q < 0.05$, FDR corrected), and adjusted R-square value was used to evaluate the power of the model.

3. Results

3.1. The trajectory of rubral branches and gross involvement in the stroke

Based on the HCP dataset, we reconstructed three pairs of rubral fibers, including the CRT, RST and DRT, and one pair of CSTs. The CRT mainly connects the red nucleus and ipsilateral frontal-parietal cortices through the internal capsule. The CRT starts from the red nucleus, and ascends through the anterior and posterior limb of the internal capsule, and terminates into ipsilateral prefrontal-parietal cortex. The DRT descends along the ipsilateral cerebral peduncle, crosses the middle line at the junction between the midbrain and pons, passes along the contralateral superior cerebellar peduncle and then terminates into the contralateral dentate. The RST originates from the red nucleus and mainly extrapolates along the dorsal part of the bilateral midbrain, pons, and medulla (Fig. 2B). The probabilistic map of each rubral branch and the CST was shown in Fig. 2C.

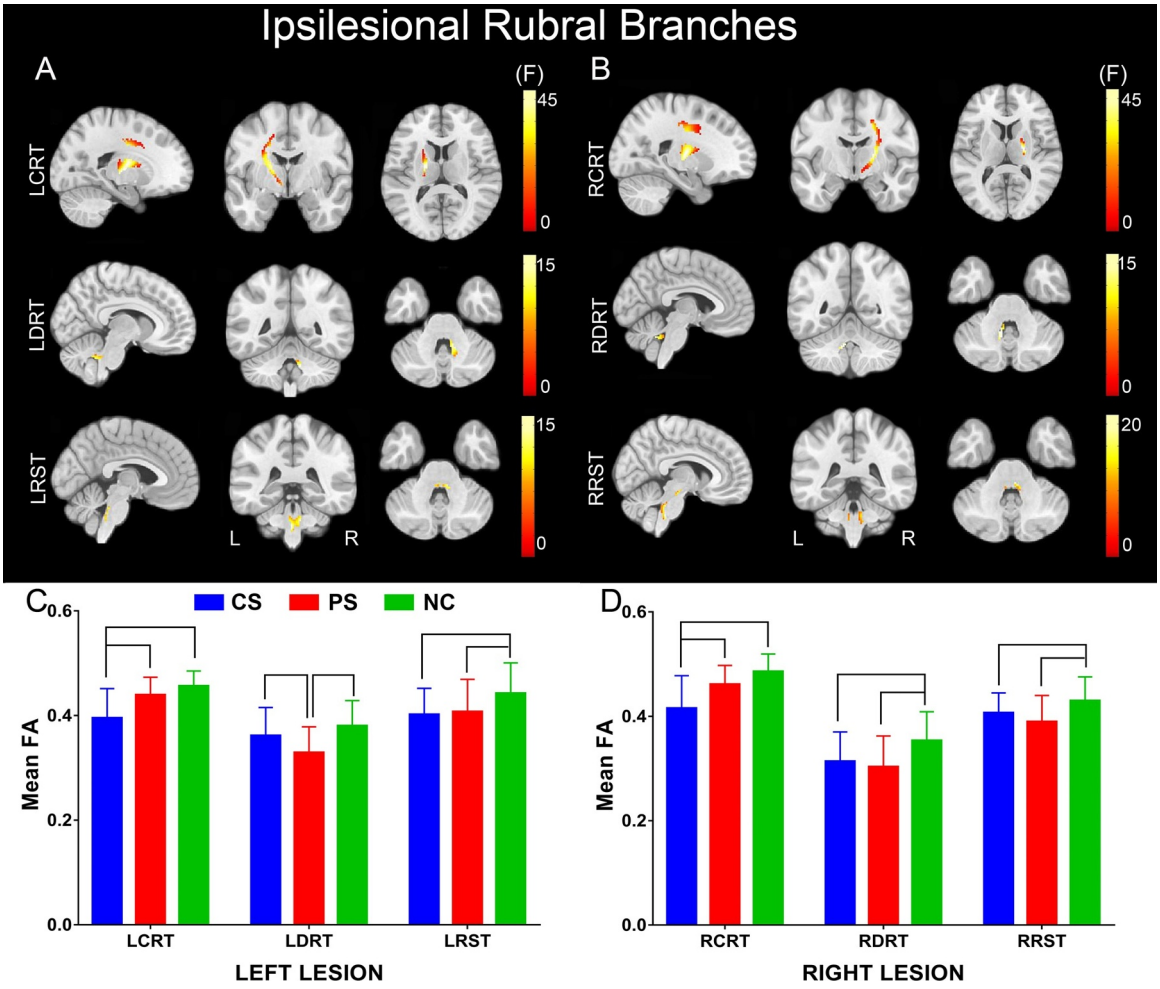

Fig. 4. Intergroup differences in FA of ipsilesional rubral branches. Voxel-wise one-way analyses of variance in FA of the ipsilesional rubral branches in patients with (A) left and (B) right infarction lesions were carried out after controlling for the effects of age, gender, and scanners (family-wise error correction, $P < 0.05$), respectively. The color map represents the F values. Post hoc analyses of the (C) left and (D) right ipsilesional rubral branches were corrected using false discovery rate ($q < 0.05$). Abbreviations: CRT = corticorubral tracts, CS = capsular stroke, DRT = dentatorubral tracts, FA = fractional anisotropy, NC = normal control, PS = pontine stroke, RST = rubrospinal tracts.

The percentage of stroke patients with direct damage was 18.29% in the left and 14.2% in the right CRT, 0.66% in the left and 1.49% in the right DRT, and 2.67% in the left and 1.20% in the right RST (Fig. 3C).

3.2. Differences in integrity of ipsilesional rubral branches between the stroke patients and the NC

VBA analyses identified significant differences in FA of ipsilesional rubral branches in patients with left (Fig. 4A) and right (Fig. 4B) stroke lesions ($P < 0.05$, cluster-wise FWE correction). ROI-wise post hoc analyses demonstrated significantly lower FA in the ipsilesional CRT of the CS than those of the PS and NC. The ipsilesional RST of both CS and PS on both sides had significantly lower FA than those of the NC ($P < 0.05$, FDR correction). The FA values of the ipsilateral DRT of the left PS were significantly lower than those of the left CS and NC, while the ipsilateral DRT of the right CS and PS had significantly lower FA than the NC ($q < 0.05$, FDR correction) (Fig. 4C and D).

Besides, the ipsilesional CRT had significantly higher AD and RD for the CS than the PS and NC. The ipsilesional DRT had higher AD and RD for the left PS than the left CS and NC, and the ipsilesional DRT had higher AD and RD for the right PS and CS than the NC. The ipsilesional RST had higher AD for the right PS and CS than the NC, and higher RD for the PS and CS than the NC ($q < 0.05$, FDR correction) (Supplementary Table 1).

3.3. Differences in integrity of contralesional rubral branches between the stroke patients and the NC

Significant differences in FA were also shown in the contralesional rubral branches in patients with both left (Fig. 5A) and right (Fig. 5B) infarction lesions by VBA ($P < 0.05$, cluster-wise FWE correction). Further post hoc analyses found that the contralesional CRT in the left CS had significantly lower FA than the NC. The contralesional RST in both the CS and PS on both sides had significantly lower FA than the NC ($q < 0.05$, FDR correction). Finally, the FA values of the contralesional DRT of the left PS were significantly lower than those of the left CS and NC, while the contralesional DRT of the right CS and PS had significantly lower FA than the NC ($q < 0.05$, FDR correction) (Fig. 5C and D).

Besides, the contralesional CRT had higher RD for the left CS and left PS than the NC. The contralesional DRT had higher AD and RD for the left PS than the left CS and NC, and higher AD and RD for the right PS and right CS than the NC. The contralesional RST had higher RD for the left CS than the NC, and higher RD for the right PS than the NC ($q < 0.05$, FDR correction) (Supplementary Table 2).

3.4. Differences in integrity of CST between the stroke patients and the NC

Additionally, VBA analyses identified significant differences in FA of

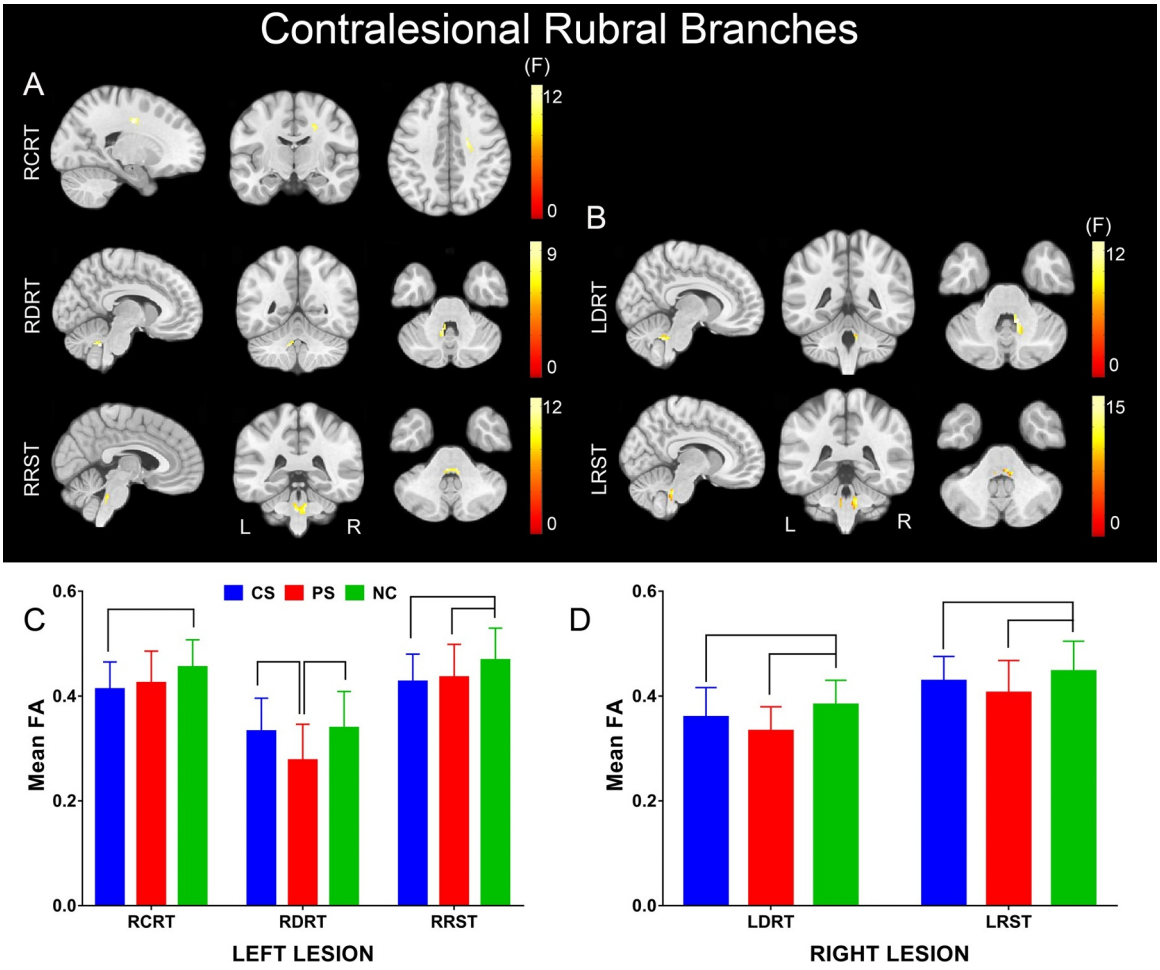

Fig. 5. Intergroup differences in FA of contralesional rubral branches. Voxel-wise one-way analyses of variance in FA of the contralesional rubral branches in patients with (A) left and (B) right infarction lesions were carried out after controlling for the effects of age, gender, and scanners (family-wise error correction, $P < 0.05$), respectively. The color map represents the F values. The region-of-interest post hoc analyses of the (C) left and (D) right contralesional rubral branches were corrected using false discovery rate ($q < 0.05$). Abbreviations: CRT = corticorubral tracts, CS = capsular stroke, DRT = dentatorubral tracts, FA = fractional anisotropy, NC = normal control, PS = pontine stroke, RST = rubrospinal tracts.(For interpretation of the references to colour in this figure legend, the reader is referred to the web version of this article.)

both ipsilesional and contralesional CST in stroke patients ($P < 0.05$, cluster-wise FWE correction). Post hoc analyses demonstrated that stroke patients had significantly lower FA in the ipsilesional and contralesional CST than the NC, and patients with right-lesion PS had significantly lower FA in the contralesional CST than the CS ($q < 0.05$, FDR correction) (Fig. 6).

3.5. The correlation between the FA of rubral branches and FMA scores

Partial correlation analyses identified significantly positive correlations between the FA of ipsilesional CST and all FMA scores in both the CS and PS ($q < 0.05$, FDR correction). Significantly positive correlations were also shown between the FA of ipsilesional CRT and the FMA total and upper extremity scores in the CS, between the FA of ipsilesional RST and the FMA total and upper extremity scores in both the CS and PS, between the FA of contralesional RST and the FMA upper extremity score in the CS, between the FA of contralesional RST and the FMA total, upper and lower extremity scores in the PS, and between the FA of contralesional DRT and FMA total, upper and lower extremity scores in the PS ($q < 0.05$, FDR correction) (Table 2).

To further elucidate whether the integrity of the rubral branches contributes independently to the severity of motor impairment that cannot be explained by the impairment of ipsilesional CST, the FA of ipsilesional CST were additionally regressed out from the partial correlation model. We still found significantly positive correlations between the FA of both ipsilesional and contralesional RST and FMA lower extremity scores in the PS ($q < 0.05$, FDR correction). Besides, we also found weak positive correlations between the FA of ipsilesional CRT/RST and FMA upper extremity score in the CS, between the FA of ipsilesional RST and FMA total score in the PS, and between the FA of contralesional RST and FMA total and upper extremity scores in the PS ($P < 0.05$ uncorrected) (Table 3).

3.6. The power of the integrity of rubral branches on explaining the individual variance in motor impairment severity

To evaluate the power of the integrity of rubral branches on explaining the individual variance in severity of motor impairment after CS and PS, a multiple linear regression model was introduced and we found that the composite FA features of all the involved rubral branches explained 39.2% of the variance in FMA scores for CS patients ($F = 6.023$, $P < 0.001$), and explained 48.8% of the variance in FMA scores for PS patients ($F = 4.817$, $P = 0.008$) (Fig. 7).

4. Discussion

In this study, we investigated the possible microstructural changes of rubral branches in chronic unilateral capsular and pontine stroke

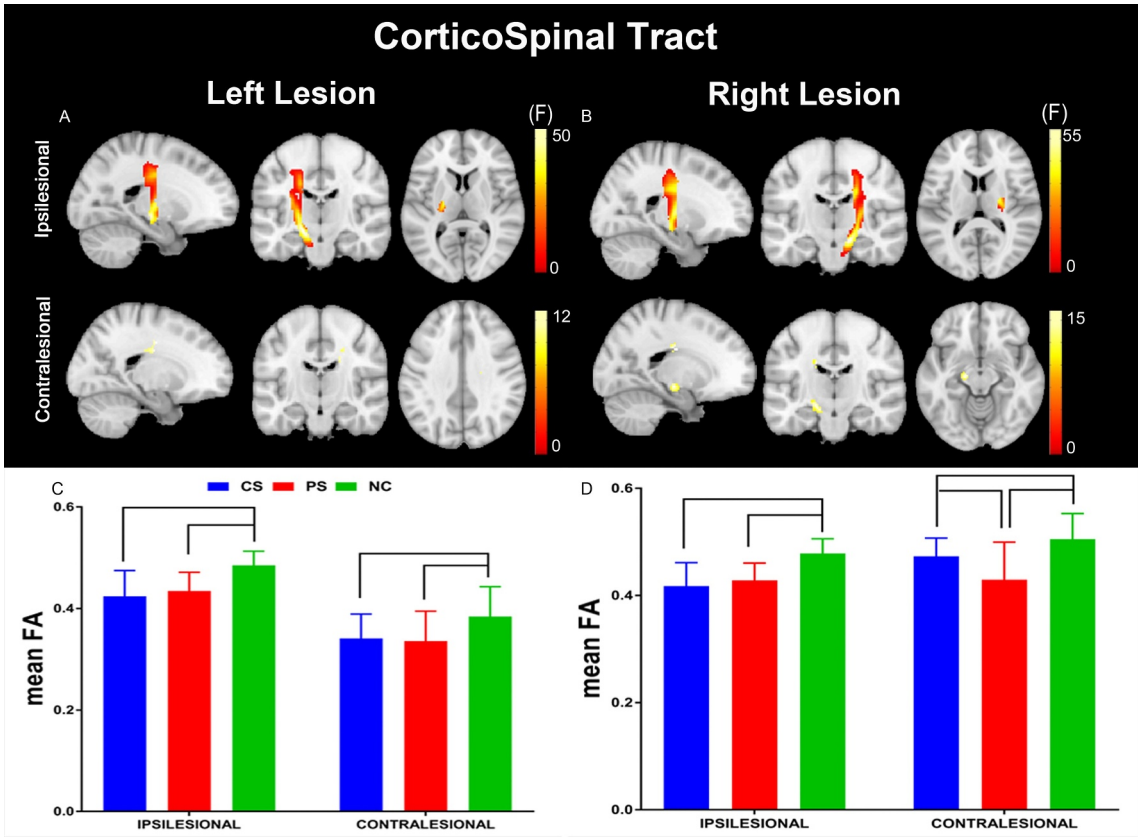

Fig. 6. Intergroup differences in FA of ipsilesional and contralesional CST. Voxel-wise one-way analyses of variance in FA of in patients with left (A) and right (B) infarction lesions were carried out after controlling for the effects of age, gender, and scanners (family wise error, $P < 0.05$), respectively. The color map represents the F values. The region-of-interest post hoc analyses of the ipsilesional and contralesional CST in patients with left (C) and right (D) infarction lesions were carried out (false discovery rate correction, $q < 0.05$). Abbreviations: ANOVA = analysis of variance, CRT = corticorubral tracts, CS = capsular stroke, DRT = dentatorubral tracts, FA = fractional anisotropy, NC = normal control, PS = pontine stroke, RST = rubrospinal tracts.

based on a fine-sculptured dMRI-based fiber-tracking procedure. We found that both the ipsilesional and contralesional rubral branches were impaired in patients with capsular and pontine stroke, and location-specific changes of these rubral branches were also present. Furthermore, the integrity of the most rubral branches were closely associated with the severity of motor impairment as revealed by FMA scores, and the association between integrity of RST and the FMA scores of lower extremity still survived after regressing out the effect of the ipsilateral CST. Finally, multiple regression model demonstrated that at least 39% of the individual variance in severity of motor impairment can be explained by the integrity of all the involved rubral branches in both the CS and PS.

Table 2
Correlations between the FA of rubral branches and motor impairment.

Group	fiber	statistics	FMA total	FMA upper extremity	FMA lower extremity	FMA hand	FMA finger
CS	IL_CRT	r	0.652	0.681	0.373	0.701	0.714
		p	**<0.001**	**<0.001**	0.027	**<0.001**	**<0.001**
	IL_RST	r	0.526	0.559	0.332	0.537	0.458
		p	**0.001**	**<0.001**	0.051	**0.001**	**0.006**
	IL_CST	r	0.735	0.693	0.686	0.723	0.694
		p	**<0.001**	**<0.001**	**<0.001**	**<0.001**	**<0.001**
	CL_RST	r	0.534	0.592	0.238	0.568	0.568
		p	0.040	**0.020**	0.393	0.027	0.027
PS	IL_RST	r	0.735	0.682	0.814	0.760	0.690
		p	**0.001**	**0.003**	**<0.001**	**<0.001**	**0.002**
	IL_CST	r	0.638	0.591	0.709	0.631	0.563
		p	**0.006**	**0.012**	**0.001**	**0.007**	**0.019**
	CL _DRT	r	0.575	0.585	0.585	0.422	0.294
		p	**0.016**	**0.014**	**0.014**	0.091	0.252
	CL_RST	r	0.639	0.571	0.757	0.685	0.660
		p	**0.006**	**0.017**	**<0.001**	**0.002**	**0.004**

Note: Partial correlation was carried out with age, gender, scanner as the nuisance covariates. Multiple comparisons were corrected using false discovery rate (FDR) methods ($q < 0.05$). Survived correlations were highlighted with **Underlined bold**. Abbreviations: CL = contralesional, CRT = corticorubral tracts, CS = capsular stroke, CST = corticospinal tract, FA = fractional anisotropy, FMA = Fugl-Meyer Assessment, IL = ipsilesional, PS = pontine stroke, RST = rubrospinal tracts.

Table 3
Correlations between the FA of rubral branches and motor impairment after additionally controlling for the effect of ipsilesional CST.

group	fiber	statistics	FMA total	FMA upper extremity	FMA lower extremity	FMA hand	FMA finger
CS	IL_CRT	r	0.264	0.365	−0.235	0.380	0.430
		p	0.131	**0.034**	0.181	**0.027**	**0.011**
	IL_RST	r	0.294	0.360	0.007	0.317	0.201
		p	0.091	**0.037**	0.967	0.068	0.255
PS	CL_RST	r	0.501	0.407	0.685	0.570	0.535
		p	**0.048**	0.118	**0.003**	**0.021**	**0.033**
	IL_RST	r	0.577	0.512	0.696	0.620	0.536
		p	**0.019**	**0.043**	**0.003**	**0.010**	**0.032**

Note: Partial correlation was carried out with age, gender, scanner, and ipsilesional FA of the CST as the nuisance covariates. Multiple comparisons were corrected using false discovery rate (FDR) methods ($q < 0.05$). **Underlined bold** represents survived after FDR correction, and only **bold** represents survived without correction for multiple comparisons. Abbreviations: CL = contralesional, CRT = corticorubral tracts, CS = capsular stroke, CST = corticospinal tract, FA = fractional anisotropy, FMA = Fugl-Meyer Assessment, IL = ipsilesional, PS = pontine stroke, RST = rubrospinal tract.

4.1. The integrity of the rubral branches plays important roles in motor dysfunction

Early studies have indicated that the cortico-rubro-spinal tracts were impaired in stroke with motor dysfunction (Ruber et al., 2012; Schulz et al., 2017; Siegel et al., 2015). In the present study, based on a larger sample size (including 93 capsular and 38 pontine stroke cases), we also found that both the ipsilesional and contralesional rubral branches were impaired in chronic stroke, and these findings can be replicated in patients with lesions in the left and right hemispheres, respectively. Moreover, the integrity of the microscopic structure of the CRT and RST was closely associated with the severity of motor impairment at the chronic stage, and the association between integrity of RST and the impairment severity of lower extremity still survived after regression out the effect of the ipsilateral CST, indicating that the RST may contribute independently to the lower limb function. Our findings further supported the notion that the integrity of the rubral branches plays important roles in motor dysfunction and recovery after stroke (Lindenberg et al., 2010; Ruber et al., 2012; Schulz et al., 2017; Siegel et al., 2015). The lower FA values along the rubral pathways can be attributed to increased radial diffusivities, which are features of chronic white matter degeneration (Qin et al., 2012) (Yu et al., 2009). The regions identified with lower FA were outside the lesion sites, especially in the DRT and RST, further suggesting the existence of secondary degeneration in addition to direct damage by stroke.

4.2. Differential involvement of rubral branches in chronic capsular and pontine stroke

One of the most important findings in the present study is the differential damage of the rubral branches after stroke. Early studies have shown that the variances in infarction location are closely associated with the types and severity of dysfunction and recovery potentials (Jiang et al., 2017). A recent voxel-based morphometry study also identified that capsular and pontine stroke induced different types of structural damage and reorganization of brain gray matter, even in brain regions outside of the lesion (Jiang et al., 2017). However, the infarction locations of previous studies about rubral pathways were heterogeneous across subjects and thus do not illustrate whether the patterns of microscopic damage of the rubral branches are dependent on the locations of the infarctions. Thus, the present study recruited two types of patients with restricted subcortical stroke, capsular stroke and pontine stroke, which directly clipped the supra-rubral and infra-rubral motor pathways, respectively. We found that the ipsilesional CRT was selectively impaired by supra-rubral capsular infarction lesions, while the bilateral RST and contralesional CRT were damaged by both capsular and pontine stroke, and these patterns consistently existed in patients with left- and right-hemispheric lesions, respectively. Finally, the ipsilesional and contralesional DRT were consistently impaired in all pontine stroke cases with both left- and right-sided lesions. The DRT was also impaired in capsular stroke with right lesions, but there was no evidence of impairment of DRT in capsular stroke with left lesions.

The selective impairment of the ipsilesional CRT in the capsular infarction was consistent with a recent study showing that the gray matter volume of the ipsilesional sensory-motor cortex was reduced in only capsular stroke rather than in pontine stroke (Jiang et al., 2017). The relatively intact integrity of the CRT in pontine stroke may be explained by that the lesion locations are far from the CRT and the transsynaptic retrograde degeneration is much slower in the central nervous system of humans (Dinkin, 2017). It is also interesting to note that the FA of the ipsilesional CRT of capsular stroke was positively associated with the severity of motor impairment. Combined with early studies (Peters et al., 2018), our findings indicate that the integrity of ipsilesional CRT may contribute to residual motor impairment.

The RST derives from the magnocellular of the red nucleus and crosses and descends to the contralateral spinal cord (Humphrey et al., 1984), which is closely associated with proximal gross movement controls in human, such as promoting extension and inhibiting flexion

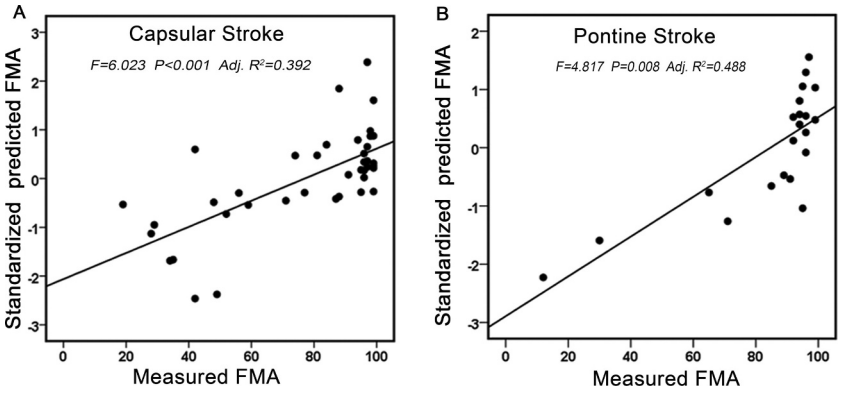

Fig. 7. The Association between the measured and predicted FMA scores using multiple regression. A multiple regression model was introduced to evaluate the power of the integrity of all involved rubral branches on explaining the individual variance in severity of motor impairment in the capsular stroke (A) and pontine stroke (B), respectively. Abbreviations: FMA = Fugl-Meyer Assessment, FA = fractional anisotropy.

(Cahill-Rowley and Rose, 2014). It should be noted that in our fiber-tracking results, the "RST" also comprises a part of fibers that connect the red nucleus and ipsilateral inferior olive nucleus (Onen et al., 2018), which is correlated with motor coordination and learning (Owen et al., 2017). In contrast to the CRT, the bilateral RST was impaired in both the unilateral capsular and pontine stroke; furthermore, the integrity of the RST was significantly correlated with motor impairment, and the correlation still survived after controlling for the contribution of ipsilesional CST damage. Our findings were consistent with a recent study showing lower FA in the RST of chronic stroke individuals and a significant correlation between the FA of RST and hand impairment severity (Owen et al., 2017). Furthermore, most of the involved RST voxels are outside the lesion location (see Fig. 3), indicating that both the direct and indirect damages of the RST can induce motor dysfunction. It should be noted that we still found significantly positive correlations between the FA of both ipsilesional and contralesional RST and FMA lower extremity scores even after controlling for the ipsilesional CST damages. It should be noted that we still found significantly positive correlations between the FA of both ipsilesional and contralesional RST and FMA lower extremity scores after regressing out the FA of ipsilesional CST. Thus, we speculated that the RST may contribute independently to the residual motor impairment that cannot be explained by the impairment of ipsilesional CST, especially for the lower limbs. This hypothesis was consistent with a recent study showing that alternate corticofugal motor fibers and CST contributed independent and synergistic role for the residual motor output (Schulz et al., 2017).

The DRT is one of the main efferent pathways of the cerebellum. It emits from the dentate nucleus through the superior cerebellar peduncle, intersecting in the midbrain, and ending in the contralateral red nucleus (Petersen et al., 2018). Because the DRT is the major pathway that transfers information between the cerebrum and cerebellum, it relates to many functions of the cerebellum, such as voluntary movements and fine motor skills (Mottolese et al., 2013). In the current study, we found that the FA values of ipsi- and contralesional DRT were significantly lower in patients with both left and right unilateral pontine stroke and in those with right unilateral capsular stroke. The impairment of the DRT found in the present study can explain the early reports of reduced GMV in the cerebellum (Jiang et al., 2017) and disrupted contralesional cerebrocerebellar connectivity in pontine stroke (Lu et al., 2011). The DRT and the RST are the important anatomical components of the Guillain-Mollaret Triangle (GMT), which forms a feedback loop connected to the brain stem and cerebellum to control the motor activity of the spinal cord (Smets et al., 2017) .Thus, the impairment of RST would cause a secondary degeneration of the DRT. In addition, supratentorial brain damage could induce a reduction in metabolic activity and blood flow of the contralesional cerebellum (named crossed cerebellar diaschisis) (Baron et al., 1981), which can also induce rupture of the corticopontocerebellar tract (Feeney and Baron, 1986; Kim et al., 1997; Tien and Ashdown, 1992). We also found a significant positive correlation between the integrity of contralesional DRT and the motor impairment. However, the correlation was not evident after controlling for the effect of the CST impairment. The possible explanation may be that the impairment of the DRT was indirect and the degeneration of the DRT was too mild. It should be noted that the DRT damages in unilateral capsular stroke in the left and right hemispheres were not consistent, which may be caused by the relatively mild deficit in motor function of the recruited patients in the present study, which should be validated in the future.

4.3. The contralesional rubral branches are indirectly involved in patient with chronic stroke

Another important finding was that the contralesional rubral branches, although not directly involved, also demonstrated lower white matter FA in both the unilateral capsular and pontine stroke. Early studies reported that the FA of contralesional cortico-spinal tracts (CST) was lower and a significant association between the FA of the contralesional CST and motor skills was identified in chronic stroke patients (Ruber et al., 2012; Schaechter et al., 2009). Moreover, brain-computer interface (BCI) training after stroke could enhance the FA of contralesional CST, and the increases in FA were correlated with improvements in finger dexterity (Atasoy et al., 2016). In the present study, we further found that the integrities of the contralesional CRT and RST were significantly associated with severity of motor impairment at the chronic stage, and the correlations still survived after controlling for the contribution of ipsilesional CST damage. Thus, these findings suggest that the integrity of the contralesional rubral branches may also contribute to individual residual motor impairment after stroke.

Several limitations should be noted in the present study. First, only 21 patients with left PS and 17 patients with right PS were included in the present study. The relatively small sample size of pontine stroke might be the cause of the missing correlation between the integrity of contralesional CRT/DRT and motor impairment. Second, the cross-sectional design in the present study cannot reveal the dynamic evolution of the integrity of the rubral pathway caused by stroke and thus cannot elucidate the contribution of reorganization of the rubral branches on the motor recovery. Third, Fugl-Meyer assessment may be not a sensitive measure to evaluate the functional impairment caused by disrupted rubral branches, which can partly explain the missing association between the integrity of DRT and FMA, and explain the missing associations for many other metrics after controlling for the effect of CST. Finally, most patients enrolled in the present study had mild motor impairment, thus the association between the FA of rubral branches and FMA scores found in the present study may not be generalized to whom had severe motor impairment.

In summary, differential impairment of rubral branches was found in patients with chronic capsular and pontine stroke; furthermore, the integrity of the rubral branches can explain the induvial variance in severity of motor impairment in both chronic capsular and pontine stroke, which cannot be completely explained by the impairment of corticospinal tract. Our findings indicate that the rubral branches may contribute independently to the residual motor output in individuals after stroke.

Funding

This work was supported by the National Key Research and Development Program of China (2018YFC1314300 and 2017YFC0909201), and the Natural Science Foundation of China (81971599, 81771818, 81425013, 81601472, 81601467 and 81871327), and Natural Science Foundation of Tianjin City (19JCYBJC25100).

Acknowledgments

The authors thank all colleagues in diagnosing, recruiting and collecting the data in the present study.

Supplementary materials

Supplementary material associated with this article can be found, in the online version, at doi:10.1016/j.nicl.2019.102090.

References

Atasoy, S., Donnelly, I., Pearson, J., 2016. Human brain networks function in connectome-specific harmonic waves. Nat. Commun. 7, 10340.
Baron, J., Bousser, M., Comar, D., Castaigne, P., 1981. "Crossed cerebellar diaschisis" in human supratentorial brain infarction. Trans. Am. Neurol. Assoc. 105, 459–461.
Cacciola, A., Milardi, D., Basile, G.A., Bertino, S., Calamuneri, A., Chillemi, G., Paladina, G., Impellizzeri, F., Trimarchi, F., Anastasi, G., Bramanti, A., Rizzo, G., 2019. The cortico-rubral and cerebello-rubral pathways are topographically organized within the human red nucleus. Sci. Rep. 9, 12117.

Cahill-Rowley, K., Rose, J., 2014. Etiology of impaired selective motor control: emerging evidence and its implications for research and treatment in cerebral palsy. Dev. Med. Child Neurol. 56, 522–528.
Cheng, B., Forkert, N.D., Zavaglia, M., Hilgetag, C.C., Golsari, A., Siemonsen, S., Fiehler, J., Pedraza, S., Puig, J., Cho, T.H., Alawneh, J., Baron, J.C., Ostergaard, L., Gerloff, C., Thomalla, G., 2014. Influence of stroke infarct location on functional outcome measured by the modified rankin scale. Stroke 45, 1695–1702.
Dinkin, M., 2017. Trans-synaptic retrograde degeneration in the human visual system: slow, silent, and real. Curr. Neurol. Neurosci. Rep. 17, 16.
Feeney, D., Baron, J., 1986. Diaschisis. Stroke 17, 817–830.
Glasser, M.F., Smith, S.M., Marcus, D.S., Andersson, J.L., Auerbach, E.J., Behrens, T.E., Coalson, T.S., Harms, M.P., Jenkinson, M., Moeller, S., Robinson, E.C., Sotiropoulos, S.N., Xu, J., Yacoub, E., Ugurbil, K., Van Essen, D.C., 2016. The human connectome project's neuroimaging approach. Nat. Neurosci. 19, 1175–1187.
Glasser, M.F., Sotiropoulos, S.N., Wilson, J.A., Coalson, T.S., Fischl, B., Andersson, J.L., Xu, J., Jbabdi, S., Webster, M., Polimeni, J.R., Van Essen, D.C., Jenkinson, M., Consortium, W.U.-M.H., 2013. The minimal preprocessing pipelines for the human connectome project. Neuroimage 80, 105–124.
Habas, C., Cabanis, E.A., 2006. Cortical projections to the human red nucleus: a diffusion tensor tractography study with a 1.5-T MRI machine. Neuroradiology 48, 755–762.
Habas, C., Cabanis, E.A., 2007. Cortical projection to the human red nucleus: complementary results with probabilistic tractography at 3 T. Neuroradiology 49, 777–784.
HUMPHREY, D.R., GOLD, R., REED, D.J., 1984. Sizes, laminar and topographic origins of cortical projections to the major divisions of the red nucleus in the monkey. J. Comp. Neurol. 225, 75–94.
Jiang, L., Liu, J., Wang, C., Guo, J., Cheng, J., Han, T., Miao, P., Cao, C., Yu, C., 2017. Structural alterations in chronic capsular versus pontine stroke. Radiology 285, 214–222.
Kim, H., Lee, H., Jung, K.I., Ohn, S.H., Yoo, W.K., 2018. Changes in diffusion metrics of the red nucleus in chronic stroke patients with severe corticospinal tract injury: a preliminary study. Ann. Rehabil. Med. 42, 396–405.
Kim, S., Choi, C., Yoon, B., Chung, J., Roh, J., Lee, M., Koh, C., 1997. Crossed-cerebellar diaschisis in cerebral infarction: technetium-99m-HMPAO SPECT and MRI. J. Nucl. Med. 38, 14–19.
Lemon, R.N., 2016. Cortical projections to the red nucleus and the brain stem in the rhesus monkey. Brain Res. 1645, 28–30.
Lindenberg, R., Renga, V., Zhu, L.L., Betzler, F., Alsop, D., Schlaug, G., 2010. Structural integrity of corticospinal motor fibers predicts motor impairment in chronic stroke. Neurology 74, 280–287.
Lotze, M., Beutling, W., Loibl, M., Domin, M., Platz, T., Schminke, U., Byblow, W., 2012. Contralesional motor cortex activation depends on ipsilesional corticospinal tract integrity in well-recovered subcortical stroke patients. Neurorehabil. Neural Repair 26, 594–603.
Lu, J., Liu, H., Zhang, M., Wang, D., Cao, Y., Ma, Q., Rong, D., Wang, X., Buckner, R.L., Li, K., 2011. Focal pontine lesions provide evidence that intrinsic functional connectivity reflects polysynaptic anatomical pathways. J. Neurosci. 31, 15065–15071.
Maier-Hein, K.H., Neher, P.F., Houde, J.C., Cote, M.A., Garyfallidis, E., Zhong, J., Chamberland, M., Yeh, F.C., Lin, Y.C., Ji, Q., Reddick, W.E., Glass, J.O., Chen, D.Q., Feng, Y., Gao, C., Wu, Y., Ma, J., Renjie, H., Li, Q., Westin, C.F., Deslauriers-Gauthier, S., Gonzalez, J.O.O., Paquette, M., St-Jean, S., Girard, G., Rheault, F., Sidhu, J., Tax, C.M.W., Guo, F., Mesri, H.Y., David, S., Froeling, M., Heemskerk, A.M., Leemans, A., Bore, A., Pinsard, B., Bedetti, C., Desrosiers, M., Brambati, S., Doyon, J., Sarica, A., Vasta, R., Cerasa, A., Quattrone, A., Yeatman, J., Khan, A.R., Hodges, W., Alexander, S., Romascano, D., Barakovic, M., Auria, A., Esteban, O., Lemkaddem, A., Thiran, J.P., Cetingul, H.E., Odry, B.L., Mailhe, B., Nadar, M.S., Pizzagalli, F., Prasad, G., Villalon-Reina, J.E., Galvis, J., Thompson, P.M., Requejo, F.S., Laguna, P.L., Lacerda, L.M., Barrett, R., Dell'Acqua, F., Catani, M., Petit, L., Caruyer, E., Daducci, A., Dyrby, T.B., Holland-Letz, T., Hilgetag, C.C., Stieltjes, B., Descoteaux, M., 2017. The challenge of mapping the human connectome based on diffusion tractography. Nat. Commun. 8, 1349.
Meola, A., Comert, A., Yeh, F.C., Sivakanthan, S., Fernandez-Miranda, J.C., 2016. The nondecussating pathway of the dentatorubrothalamic tract in humans: human connectome-based tractographic study and microdissection validation. J. Neurosurg. 124, 1406–1412.
Milardi, D., Cacciola, A., Cutroneo, G., Marino, S., Irrera, M., Cacciola, G., Santoro, G., Ciolli, P., Anastasi, G., Calabro, R.S., Quartarone, A., 2016. Red nucleus connectivity as revealed by constrained spherical deconvolution tractography. Neurosci. Lett. 626, 68–73.
Mottolese, C., Richard, N., Harquel, S., Szathmari, A., Sirigu, A., Desmurget, M., 2013. Mapping motor representations in the human cerebellum. Brain 136, 330–342.
Onen, M.R., Moore, K., Cikla, U., Ucer, M., Schmidt, B., Field, A.S., Baskaya, M.K., 2018. Hypertrophic olivary degeneration: neurosurgical perspective and literature review. World Neurosurg. 112, e763–e771.
Owen, M., Ingo, C., Dewald, J., 2017. Upper extremity motor impairments and microstructural changes in bulbospinal pathways in chronic hemiparetic stroke. Front. Neurol. 8, 257.
Peters, D.M., Fridriksson, J., Stewart, J.C., Richardson, J.D., Rorden, C., Bonilha, L., Middleton, A., Gleichgerrcht, E., Fritz, S.L., 2018. Cortical disconnection of the ipsilesional primary motor cortex is associated with gait speed and upper extremity motor impairment in chronic left hemispheric stroke. Hum. Brain Mapp. 39, 120–132.
Petersen, K.J., Reid, J.A., Chakravorti, S., Juttukonda, M.R., Franco, G., Trujillo, P., Stark, A.J., Dawant, B.M., Donahue, M.J., Claassen, D.O., 2018. Structural and functional connectivity of the nondecussating dentato-rubro-thalamic tract. Neuroimage 176, 364–371.
Qin, W., Zhang, M., Piao, Y., Guo, D., Zhu, Z., Tian, X., Li, K., Yu, C., 2012. Wallerian degeneration in central nervous system: dynamic associations between diffusion indices and their underlying pathology. PLoS ONE 7, e41441.
Ruber, T., Schlaug, G., Lindenberg, R., 2012. Compensatory role of the cortico-rubrospinal tract in motor recovery after stroke. Neurology 79, 515–522.
Schaechter, J.D., Fricker, Z.P., Perdue, K.L., Helmer, K.G., Vangel, M.G., Greve, D.N., Makris, N., 2009. Microstructural status of ipsilesional and contralesional corticospinal tract correlates with motor skill in chronic stroke patients. Hum. Brain Mapp. 30, 3461–3474.
Schulz, R., Park, E., Lee, J., Chang, W.H., Lee, A., Kim, Y.H., Hummel, F.C., 2017. Synergistic but independent: the role of corticospinal and alternate motor fibers for residual motor output after stroke. Neuroimage Clin. 15, 118–124.
Siegel, C.S., Fink, K.L., Strittmatter, S.M., Cafferty, W.B., 2015. Plasticity of intact rubral projections mediates spontaneous recovery of function after corticospinal tract injury. J. Neurosci. 35, 1443–1457.
Smets, G., Lambert, J., Tijssen, M., Mai, C., Decramer, T., Vandenberghe, W., Van Loon, J., Demaerel, P., 2017. The dentato-rubro-olivary pathway revisited: new MR imaging observations regarding hypertrophic olivary degeneration. Clin. Anat. 30, 543–549.
Sotiropoulos, S.N., Jbabdi, S., Xu, J., Andersson, J.L., Moeller, S., Auerbach, E.J., Glasser, M.F., Hernandez, M., Sapiro, G., Jenkinson, M., Feinberg, D.A., Yacoub, E., Lenglet, C., Van Essen, D.C., Ugurbil, K., Behrens, T.E., Consortium, W.U.-M.H., 2013. Advances in diffusion MRI acquisition and processing in the human connectome project. Neuroimage 80, 125–143.
Sterr, A., Shen, S., Szameitat, A., Herron, K., 2010. The role of corticospinal tract damage in chronic motor recovery and neurorehabilitation: a pilot study. Neurorehabil. Neural Repair 24, 413–419.
Stinear, C., Barber, P., Smale, P., Coxon, J., Fleming, M., Byblow, W., 2007. Functional potential in chronic stroke patients depends on corticospinal tract integrity. Brain 130, 170–180.
Teipel, S.J., Reuter, S., Stieltjes, B., Acosta-Cabronero, J., Ernemann, U., Fellgiebel, A., Filippi, M., Frisoni, G., Hentschel, F., Jessen, F., Kloppel, S., Meindl, T., Pouwels, P.J.W., Hauenstein, K.H., Hampel, H., 2011. Multicenter stability of diffusion tensor imaging measures: a European clinical and physical phantom study. Psychiatry Res. 194, 363–371.
Tien, R., Ashdown, B., 1992. Crossed cerebellar diaschisis and crossed cerebellar atrophy: correlation of MR findings, clinical symptoms, and supratentorial diseases in 26 patients. AJR Am. J. Roentgenol. 158, 1155–1159.
Ugurbil, K., Xu, J., Auerbach, E.J., Moeller, S., Vu, A.T., Duarte-Carvajalino, J.M., Lenglet, C., Wu, X., Schmitter, S., Van de Moortele, P.F., Strupp, J., Sapiro, G., De Martino, F., Wang, D., Harel, N., Garwood, M., Chen, L., Feinberg, D.A., Smith, S.M., Miller, K.L., Sotiropoulos, S.N., Jbabdi, S., Andersson, J.L., Behrens, T.E., Glasser, M.F., Van Essen, D.C., Yacoub, E., Consortium, W.U.-M.H., 2013. Pushing spatial and temporal resolution for functional and diffusion MRI in the human connectome project. Neuroimage 80, 80–104.
Van Essen, D.C., Smith, S.M., Barch, D.M., Behrens, T.E., Yacoub, E., Ugurbil, K., Consortium, W.U.-M.H., 2013. The WU-Minn human connectome project: an overview. Neuroimage 80, 62–79.
Yeh, F.C., W.V., T.W.Y., 2010. Generalized q-sampling imaging. IEEE Trans. Med. Imaging 29, 1626–1635.
Yeh, F.C., Verstynen, T.D., Wang, Y., Fernandez-Miranda, J.C., Tseng, W.Y., 2013. Deterministic diffusion fiber tracking improved by quantitative anisotropy. PLoS ONE 8, e80713.
Yeo, S.S., Jang, S.H., 2010. Changes in red nucleus after pyramidal tract injury in patients with cerebral infarct. NeuroRehabilitation 27, 373–377.
Yu, C., Zhu, C., Zhang, Y., Chen, H., Qin, W., Wang, M., Li, K., 2009. A longitudinal diffusion tensor imaging study on Wallerian degeneration of corticospinal tract after motor pathway stroke. Neuroimage 47, 451–458.